Chapter 4

Low-cost chemically treated sugarcane bagasse for removal of cationic, anionic, and neutral dyes from aqueous solution

4.1 Introduction

The rise in population, industrial development, and agricultural sector growth have enhanced the need for fresh water, resulting in a severe problem of water scarcity. Moreover, the available fresh water is being contaminated for the above-stated reasons. There should be a balance between maintaining existing water reserves and consumption according to our needs. Lellis et al. (2019). Currently, worldwide, many living organisms are severely affected by water pollution, and it is a severe problem that causes a lot of damage to our ecosystem. Industrial water pollution is one of the significant causes of the pollution of the aqueous system. The most important source of wastewater is the textile and dye industries, where the major component of sewage is organic synthetic dyes used as a colouring or dyeing agent. More than a million tons of dyes are created yearly by the textile industry, and they also produce various other chemicals which cause pollution, Koduru et al. (2019). One well-known water-intensive process that raises severe environmental concerns is dying. Typically, synthesised organic compounds are utilised as dyes in commercial colouring applications, Berradi et al. (2019). They are divided into three groups according to charge: cationic (like methylene blue, MB), anionic (like methyl orange, MO), and neutral (like neutral red, NR). Their reactivity varies depending on which group they belong to Benkhaya et al. (2020). Because the dying process is ineffective, roughly 10–20% of dyes are dumped into water bodies as industrial waste, which harms marine life. Therefore, removing these pollutants from the water before disposing of them is essential, Patel et al. (2022). Another issue with dyes is that to make them durable, these molecules are given extra stability during production, Dindorkar et al. (2022). Thus, it is challenging to remove the hazardous dyes naturally. Adsorption, filtration, and degradation often employ techniques to eliminate dyes from aquatic environments or transform them into beneficial or less hazardous byproducts, Dutta et al. (2021). Adsorption, filtration, and

degradation often employ techniques to eliminate dyes from aquatic environments or transform them into beneficial or less hazardous byproducts, Biswal et al. (2021).

Sugarcane bagasse (SCB) is one of the sugarcane industry's bi-products, consisting of cellulose, hemicellulose, lignin, and other materials such as wax in small quantities, Prasad et al. (2020). SCB has been applied for many purposes, including producing several materials, including cellulose, bioethanol, hemicellulose, composites, methane, etc. Around 40 to 50 per cent of SCB is cellulose, a glucose polymer. Other parts consist of hemicellulose, lignin and wax. A lot of researchers have done various experiments to extract them from SCB. Feng et al. (2017), isolated cellulose through successive abstractions of dewaxed SCB with H_2O_2 through ultrasonic irradiation and produced 44.7 and 45.9% cellulose and a significant amount of hemicellulose and lignin, developed an eco-friendly method to make carbon nanofibers from SCB through an ultra-sonication collective with several mechanochemical pre-treatments. Arni (2018), separated lignin from sugarcane by various methods, such as ionic liquid and alkaline means. Brienzo et al. (2009), extracted hemicellulose from hydrogen peroxide alkaline solution. This method permitted low and high lignin extraction conditions in hemicellulose. As evident from the above discussion and the easy cellulose extraction from SCB, they have attracted significant attention in water treatment. For instance, Bai et al. (2021) prepared SCB biochar/iron oxide composite to eliminate Cr (VI) in wastewater via adsorption. The SCB biochar/iron oxide composite showed a Cr (VI) adsorption capacity of 55 mg/g under the optimised situations. Noreen et al. (2020), synthesised polymeric biocomposites of SCB and used them to remove Acid Black dye. The composite showed promising results in the elimination of acid black dye. Zhang et al. (2011), prepared SCB through the ball milling process and used it for the adsorptive removal of Congo red. It had an adsorption capacity of 38.2 mg/g of SCB for 500 ppm CR concentration. Amin (2008), synthesised activated carbon from SCB through chemical activation with H_3PO_4 followed by pyrolysis and through physical

activation in an air-free environment and used it for removal. Various activated carbons were used to eliminate reactive orange dye from water. Da Silva et al. (2011), prepared biomass from SCB through acid hydrolysis and successfully treated textile wastewater to remove reactive red-2BE dye. Tahir et al. (2012), used SCB, carbonaceous SCB and fly ash bagasse to extract malachite green dye from water. The results indicate that carbonaceous SCB showed the highest adsorption capacity compared to other bagasse. Yu et al. (2012), synthesised recyclable magnetised pyromellitic dianhydride-modified SCB with an adsorption capacity of 315.5 and 304.9 mg/g for malachite green and basic magenta dyes. Wang et al. (2020), synthesised SCB-$CaCO_3$ composite as adsorbent to eliminate crystal violet dye from wastewater. The adsorption capacity of SCB-$CaCO_3$ for crystal violet dye was 3.33 mg/mL with a removal efficiency of 97.67%. Abdelghaffar et al. (2019), showed that SCB improved the adsorption capacity of an effective, low-cost and attractive adsorbent for dye removal from wastewater.

Although there have been various studies on the adsorption of dyes using SCB and its composites, no study compares its capability to adsorb cationic, anionic, and neutral dyes. Furthermore, agricultural by-products are considered low-value products arbitrarily discarded or burned, resulting in resource loss and environmental pollution. Hence, using SCB can prove to be cost-effective. These substances generally have strong sorption capabilities toward dye molecules that are negatively or positively charged, but not both. Nonetheless, industrial wastewater typically contains a blend of several hues. Therefore, sorbents that can remove many dye types individually or concurrently are required. Very few studies have shown material that may be used to remove cationic, anionic and neutral dyes Gajera et al. (2022). This study studies this gap and presents the results for the adsorption of three dyes: cationic (MB), anionic (MO), and neutral (NR) dyes. Besides, this study helps to provide a greener method for the adsorption of textile dyes, hence helping to reduce pollution. The prepared SCB was characterised using a scanning electron microscope (morphology) and Fourier transform

infrared techniques. The study examined the impact of adsorbent dosage, contact time, pH, and concentration on the adsorption efficiency of SCB in eliminating MB, MO, and NR dyes. Kinetic and isotherm experiments were also conducted to comprehend the adsorption process better.

4.2 Materials and Methods

4.2.1 Materials

Sugarcane bagasse was purchased from a shop near Lanka, Varanasi, India. Formaldehyde (37% purity) was purchased from SRL Chemicals. MB, NR and MO dyes (99% purity) were obtained from Nice Chemicals Cochin, India. De-ionised water was obtained from the Milli-Q setup. Hydrochloric acid and sodium hydroxide were purchased from Spectro Chem Ltd. All the chemicals were used without any further purification.

4.3 Adsorbent synthesis

The SCB was collected from Lanka Gate, Varanasi, UP and washed adequately with deionised water. Then, it was dried under sunlight for 48 hours and stored overnight in an oven to eliminate the solvent organic compounds and tannins. The dried SCB was crushed into powder, and 10 g of powdered SB was treated with 1% formaldehyde in the 1:4 ratio, Kharat (2015). The mixture was heated for 24 h at 100°C. Then, the SCB treated with formaldehyde was collected and dehydrated in an oven at 100 ºC for nearly 24 h and crushed again to obtain finely powdered SCB. This was then utilised in the following adsorption experiments and characterisations.

4.4 Adsorption experiments

Adsorption experiments were performed to examine the effective removal of MB, MO, NR dyes and adsorption capacity using chemically treated SCB. Experiments were performed by altering parameters like pH, adsorbent dosage, initial dye concentration, and contact time to arrive at the optimum environments for MB, MO, and NR dye adsorption. To measure the

effect of MB, MO and NR dye concentration on the sugarcane bagasse, the solution concentration was changed from 10 to 120 ppm. The pH of MB, MO and NR dye solutions was changed from 2 to 12 to measure the effect caused by pH on MB, MO and NR dye adsorption by sugarcane bagasse. The pH adjustment was achieved using 0.1 N HCl or 0.1 N NaOH for all the experiments. The initial adsorbent dose was changed from 0.4-12 mg/L to measure the effect caused by the adsorbent dose on MB, MO and NR dye adsorption by sugarcane bagasse. The adsorbent's contact time was changed to 10 to 180 min to improve the adsorption time. Hence, adsorption capacity as well as removal efficiency was assessed from the equations

$$\text{Adsorption capacity } (q_e) = (C_i - C_e/m) \times V \quad (4.1)$$

$$\text{Removal Efficiency} = (C_i - C_e / C_i) \times 100 \quad (4.2)$$

where q_e - equilibrium adsorption capacity, C_i - MB, MO and NR dye's primary concentration, C_e - MB, MO and NR dye's equilibrium concentration, m - mass of the sugarcane bagasse, and V - volume of MB, MO and NR dye's solution.

4.4.1 Adsorption kinetics

In the beginning of the adsorption, the process modifies as time goes forward. Therefore, time is important in learning kinetics of an adsorbent's performance Kurniawati et al. (2021). The pathway which is followed during the adsorption process can be predicted by studying the kinetics of the process. In the adsorption process, the physiochemical features of the adsorbent and system parameters such as contact time determine the process's nature and pathway. The quantity of dye adsorbed at time t, denoted by q_t calculated by using the given equation:

$$\text{Adsorption capacity } (q_t) = (C_i - C_t/m) \times V \quad (4.3)$$

where q_t - adsorbed ions amount per unit mass of the adsorbent in time t, m - mass of adsorbent utilized, and C_t - dye's concentration at instant t.

To examine the adsorption kinetics in this study, the linear pseudo-first-order (PFO) and the pseudo-second-order (PSO) kinetic models. The linear form of the PFO and PSO equation as given, Sahu et al. (2019).

$$\ln (q_e - q_t) = \ln q_e - k_1 t \quad (4.4)$$

$$t/q_t = 1/k_2 q_e^2 + t/ q_e \quad (4.5)$$

where q_t amount of adsorbed ions per unit adsorbent at instant t, k_1-PFO constant, and k_2 rate constant of the PSO.

4.4.2 Adsorption isotherm

The adsorption isotherms were utilized to examine the adsorption mechanism. The adsorption isotherms offer the equilibrium concentration between the adsorbed and unabsorbed phase at a specific state, Mate and Mishra (2020). Moreover, it helps to choose the adsorbents, Fakher & Imqam (2019). The Langmuir and Freundlich isotherms were select for this study. The Langmuir adsorption (monolayer adsorption) isotherm assumes that the adsorption occurs within the adsorbent at specific homogeneous positions. The linear form of the Langmuir isotherm is defined as Berizi et al. (2016).

$$C_e/q_e = 1/ q_m K_L + C_e / q_m \quad (4.6)$$

where K_L - constant for Langmuir isotherm, q_m - maximum adsorption capacity, C_e - equilibrium concentration of dye in solution. The interaction as reversible and non-ideal adsorption is characterized by Freundlich isotherm. This isotherm model describes the adsorption process are multilayer sorption procedure of ions that bind on the surface of a heterogeneous adsorbent,

exponential distribution of active sites and energy onto the adsorbent surface. The linear type of the equation of Freundlich isotherm is defined as:

$$\ln q_e = \ln K_F + 1/n \quad \ln C_e \qquad (4.7)$$

where $1/n$- intensity and K_F - Freundlich coefficient.

4.5 Adsorbent fabrication cost analysis

Any adsorbent's production costs are a crucial factor in whether or not it can be commercially used in large-scale field applications. Feedstock, chemical, and reagent costs, as well as electricity costs, are all included in the fabrication cost analysis. Using the following equations, the adsorbent's manufacturing cost (INR/kg) was calculated, Das et al. (2023).

$$\text{Power utilized (kwh)} = \text{Power (W)} \times \text{Time(min)}/1000 \times 60 \qquad (4.8)$$

$$\text{Energy cost (INR)} = \text{Power consumed (kwh)} \times \text{Electricity cost (INR/kwh)}/1000 \times 60 \qquad (4.9)$$

$$\text{Chemical cost (INR)} = \text{Chemical required (kg)} \times \text{Unit cost (INR/kg} \qquad (4.10)$$

4.6 Characterization techniques

A Perkin Elmer Fourier transformation spectroscopy (FTIR) spectrometer (USA) was used for an adsorbent IR spectrograph. Optical microscopy was performed using a USB camera (0-500x) to study the morphological characteristics of the adsorbent. The amount of MB dye concentrations was evaluated using a UV-Vis spectrophotometer by making a calibration curve, and for pH monitoring, an Eutech PC2700 multiparameter device (Shimadzu, Japan) was used. The characteristic absorbance of MB, MO, and NR dyes was at 665, 465, and 534 nm, respectively, and was selected to examine the decolourisation through adsorption.

4.7 Results and Discussions

4.7.1 Characterization studies

The optical images of SCB after chemical treatment and after adsorption of methylene blue, neutral red and methyl orange are shown in Fig. 4.1. After the adsorption of respective dyes, dye adhesion occurred on the SCB surface, confirmed by the change of colour. Further, there

was no contaminant, as seen from the optical images. The size of particles varies and can be controlled by the used depending on the crushing time and conditions.

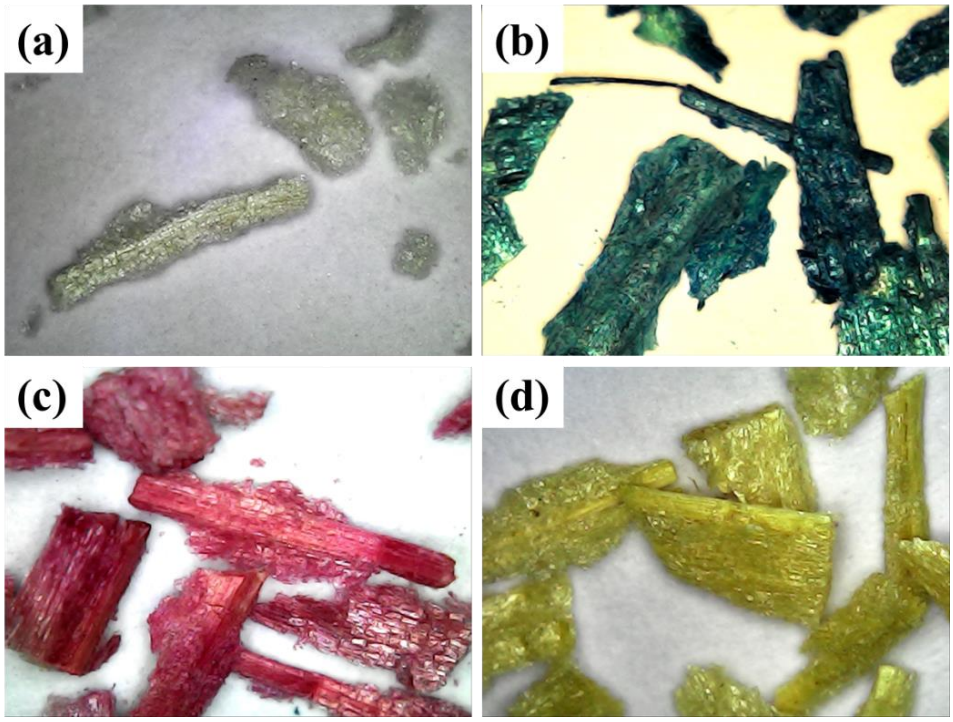

Fig. 4.1 Optical images of SCB (a) after chemical treatment, (b) after adsorption of methylene blue, (c) after adsorption of neutral red and (d) after adsorption of methyl orange

Fig. 4.2 shows the SEM images and EDS of treated SCB before and after the adsorption of various dyes used in this study. The SEM image of SCB shows the uneven, rough surface of SBA after adsorption compared to before. The number of canals was seen clearly in an initial case, i.e. before adsorption, and after adsorption, the canal was filled with Dye contaminant molecules. The elemental analysis revealed that SCB contained carbon, nitrogen, oxygen, silicon and calcium elements. After adsorption, the elements that are present in dyes were also detected.

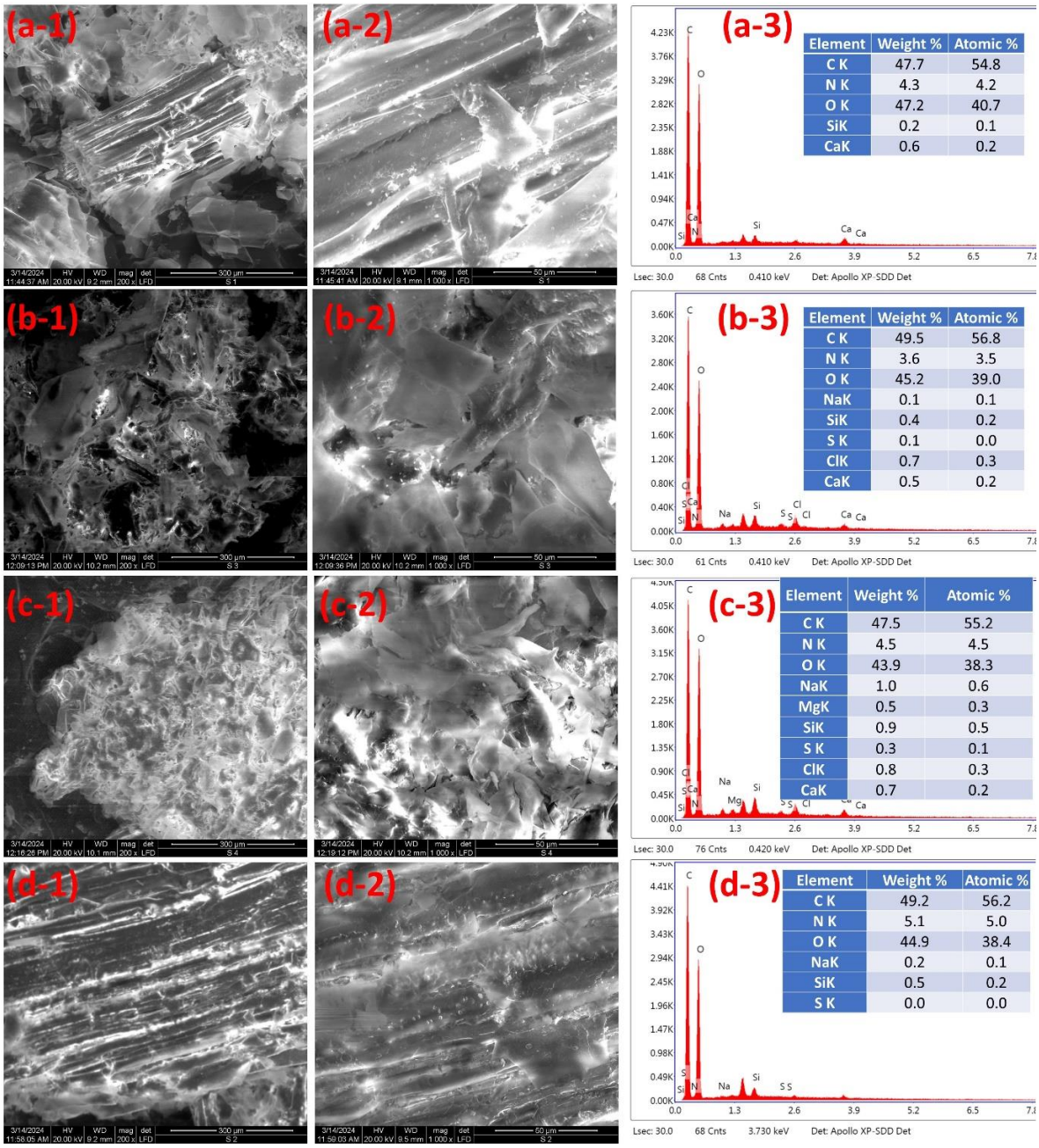

Fig. 4.2 SEM images and EDS of SCB (a) after chemical treatment, (b) after adsorption of MB dye, (c) after adsorption of NR dye and (d) after adsorption of MO dye

The details on the chemical functional group can be obtained from FTIR spectroscopy. The FTIR spectra of raw and chemically treated SCB are shown in Fig. 4.3. The bands at and around 3500 cm^{-1} were attributed to the O-H stretching intramolecular hydrogen bonds for cellulose, Viera et al. (2006). The bands at and around 2800 and 1730 cm^{-1} were attributed to C-H

stretching and C-O stretching vibrations, respectively, for the acetyl and ester linkages in lignin, hemicellulose, and pectin, Garside & Wyeth (2003). The stretching vibrations at 1620-1649, 1512, and 1595 cm^{-1} were attributed to the aromatic ring present in lignin. The bands at 1250 cm^{-1} were attributed to C–O out-of-plane stretching vibrations in lignin's aryl group, Kumar et al. (2020). The effect of this chemical purification can be observed through spectral bands visible at 1512 and 1250 cm^{-1}. It was observed that after chemical treatment, the bands became sharper.

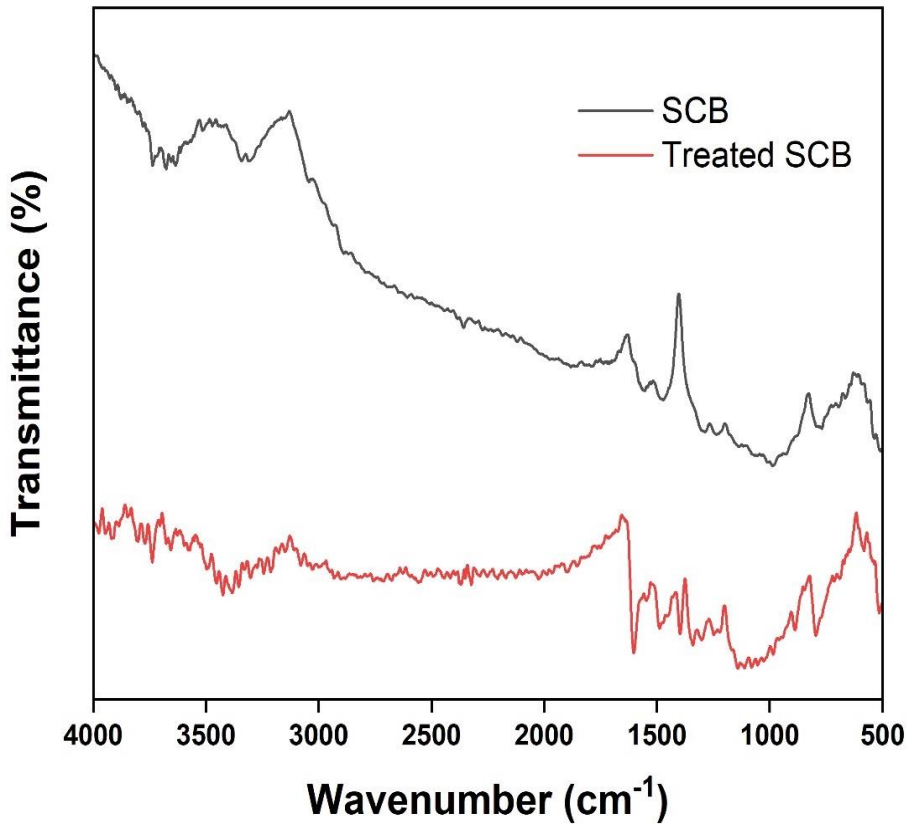

Fig. 4.3 FTIR spectrum of sugarcane bagasse before and after chemical treatment

The X-ray diffractogram pattern of SCB is shown in Fig. 4.4. The diffractogram pattern showed peaks at 14.6°, 16.5° and 22.8°, which have been observed earlier by other researchers, Oudiani et al. (2011). Based upon the diffractogram pattern, the crystallinity index of SCB was obtained at 57%, as calculated using the empirical method of Segal et al. (1959). The crystallinity in treated SCB was due to the cellulose content in the SCB.

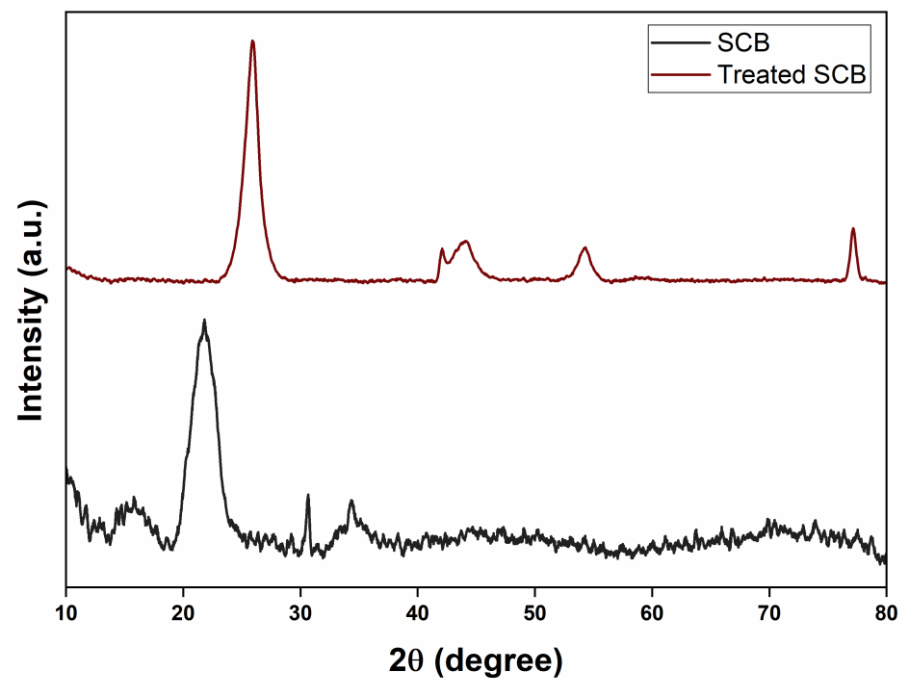

Fig. 4.4 X-ray pattern of SCB and treated SCB

Fig. 4.5 displays the TGA data, which were used to examine the mass losses of the treated SCB before and after adsorption as a function of temperature. The data indicate that the SCB have a negligible % mass loss of 0.8% between 20°C and 100°C. Since the temperature during the adsorption process is not very high, the synthesised material will have sufficient operability over the application's temperature range.

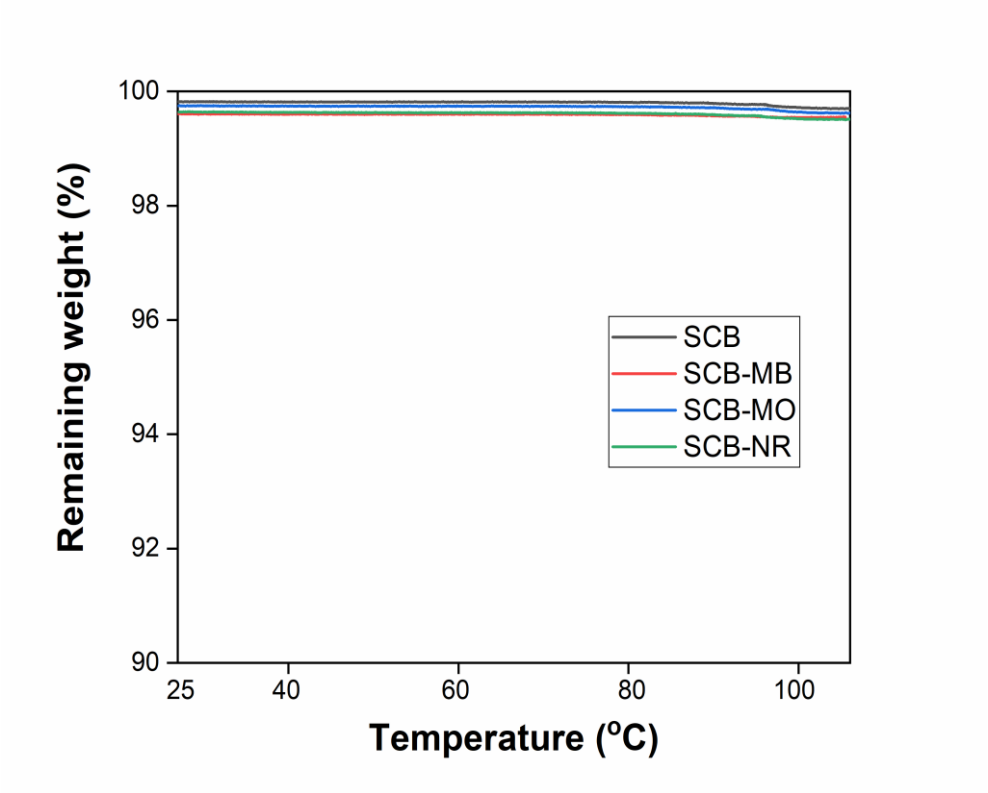

Fig. 4.5 TGA plots of SCB before and after adsorption

4.8 Adsorption experiments

A series of adsorption experiments were accomplished by changing one parameter at a time and keeping others constant. The effects of those parameters on the process are explained in the following sub-units.

4.8.1 Effect of adsorbent dose

To eliminate MB, MO and NR dye with sugarcane bagasse, the effect of the adsorbent dose (0.4-12 g/L) was studied, keeping other parameters constant (Fig. 4.6). The removal efficiency of MB, MO and NR dye increased with adsorbent doses from 0.4 to 12 g/L. The removal efficiency also showed an increment with increasing adsorbent dose, which was attributed to increased accessibility of adsorption sites Even though the increase in the removal efficiency of dyes showed great difference between each other, this was according to the capability of the

respective dyes in accordance to the sugarcane bagasse. As observed from (Fig. 4.4), the MB dye showed better adsorption with SCB as the adsorbent dose, whereas MO showed the least adsorption, even smaller than neutral red with increasing adsorbent dose. Whereas the adsorption capacity decreases with an increase in dose, it decreases with an increase in removal efficiency as well. The maximum adsorption capacity is also shown by MB (98.2%). NR depicts the least adsorption capacity. Maximum adsorption capacity depicted by NR (52.4%) results.

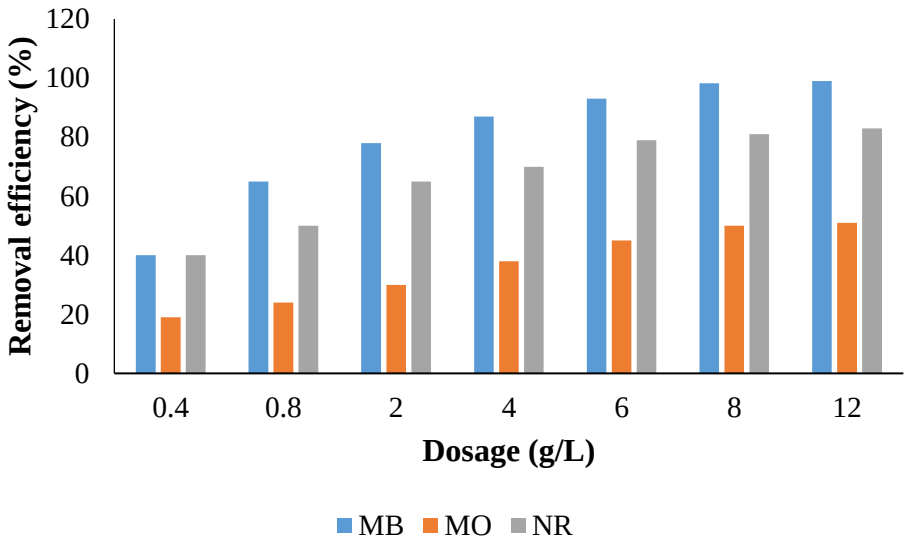

Fig. 4.6 Removal efficiency of MB, MO and NR dyes using SCB with variable adsorbent dose. (Initial dye concentrations: 50 ppm, contact time: 120 min, and pH: 10-MB, 8-NR, 12-MO)

4.8.2 Effect of pH

To study the consequence of MB, MO, and NR dye solution pH on the adsorption removal efficiency of SCB adsorbent, the pH of the solution was varied from 2 to 12 while keeping other parameters fixed. With increased MB dye solution pH, the removal efficiency amplified from 45.1 % to 99 % with extreme elimination efficiency at 10 pH (Fig. 4.7). In a similar trend, with an increase in MO dye solution pH, the removal efficiency also increased from 26% to

58%, with the best elimination efficiency at 12 pH. With increased NR dye solution pH, the removal efficiency also increased from 48% to 83% with the best elimination efficiency at eight pH. The zero-point charge (ZPC) is the pH value at which the surface charge on the adsorbent is equal to zero. The ZPC value of adsorbent SBA was found to be 7.2. The net positive charge on the adsorbent is represented by a pH below the isoelectric or ZPC point, while a pH above the ZPC point represents the net negative surface charge Kerrou et al. (2021). When the pH is greater than ZPC, cation adsorption rises; when the pH is lower than ZPC, anion adsorption increases, Ponce et al. (2021). The increase in elimination efficiency with pH was due to the negative charge on the SCB, positive charge on MB dye and negative charge on MO dye, Chiao et al. (2020), These surface charges were responsible for an attractive interaction between MB dye and SCB adsorbent, resulting in a rise in the removal efficiency, Saha et al. (2023).

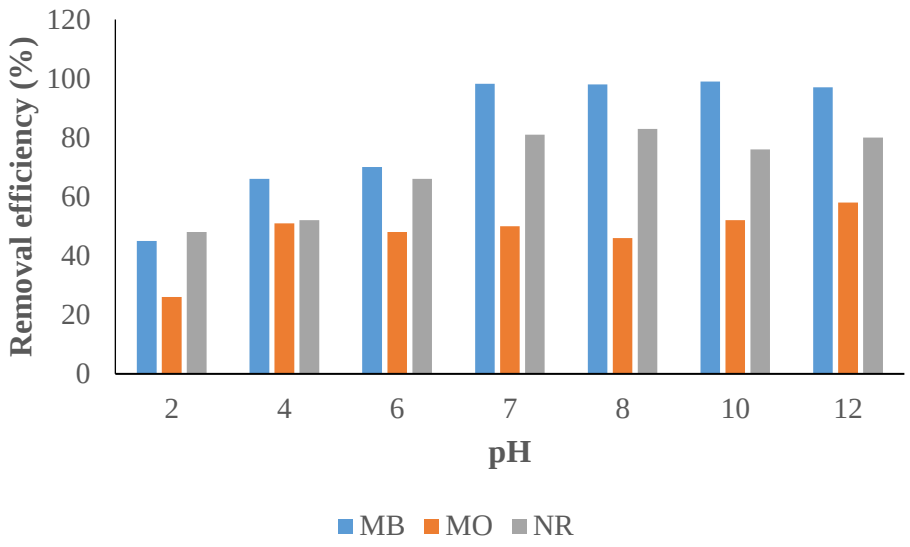

Fig. 4.7 Removal efficiency of MB, MO and NR dyes using SCB with variable pH (Adsorbent dose: 8 g L^{-1}, initial dye concentrations: 50 ppm, and contact time: 120 min)

4.8.3 Effect of Contact Time

The influence of contact time between the SCB adsorbent and MB, MO, and NR dye's removal efficiency for MB dye adsorption was examined using variable contact time while keeping

other parameters fixed. The removal efficiency increased speedily with the increase in the adsorbent's contact time, and the curve became plateau later (Fig. 4.8). The increases in removal efficiency were attributed to the initial availability of additional adsorption active sites, and as the adsorption procedure passed, the active number of sites decreased (as the adsorbent dose was fixed); hence, the curve became plateaued, Geng et al. (2018). The highest removal efficiency of MB was 98.2 % at 120 min, after which the removal efficiency and adsorption capacity plots plateau. Similar observations are also seen in other studies, Deb et al. (2023).

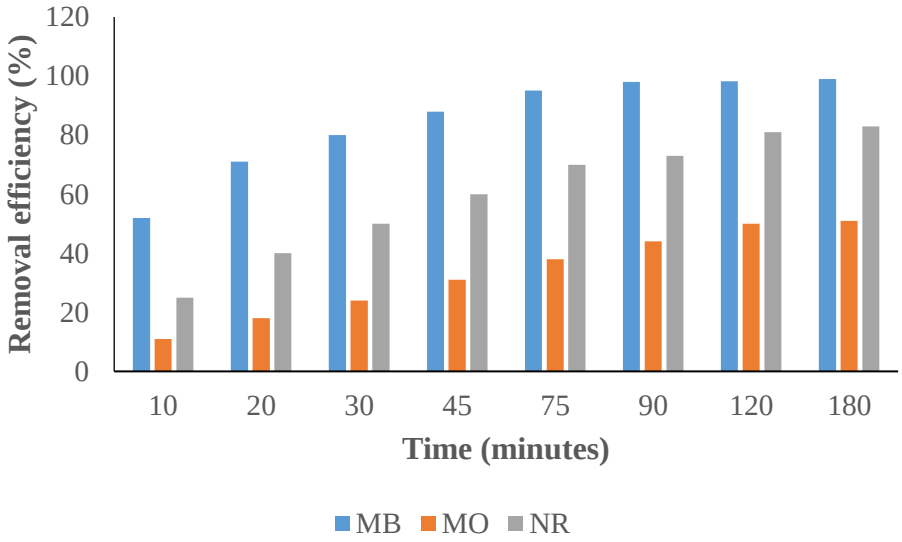

Fig. 4.8 Removal efficiency of MB, MO and NR dyes using SCB with variable contact time. (Adsorbent dose: 8 g L^{-1}, initial dye concentrations: 50 ppm, and pH: 10-MB, 8-NR, 12-MO)

4.8.4 Effect of the Initial Dye Concentration

The influence of preliminary concentration of MB, MO and NR dye on removal efficiency was examined, keeping other parameters fixed. The removal efficiency reduced as the preliminary concentration rose (Fig. 4.9). The diminished removal efficiency was most likely due to increased contact of dye with available active sites on SCB adsorbent. When the initial concentration of MB dye increased from 10 to 120 ppm, the removal efficiency showed a reduction of 99.3% to 55.1%. When the initial concentration of MO dye increased from 10 to

120 ppm, the removal efficiency showed a reduction of 52.3% to 26.8%. When the initial concentration of NR dye increased from 10 to 120 ppm, the removal efficiency showed a reduction of 84.4% to 61.2%. The removal efficiency also decreased due to the static adsorbent dose as the concentration of dye molecules increased, but the adsorbent sites were fixed; therefore, the SCB adsorbent could not hold the other dye molecules, Jahan et al. (2020).

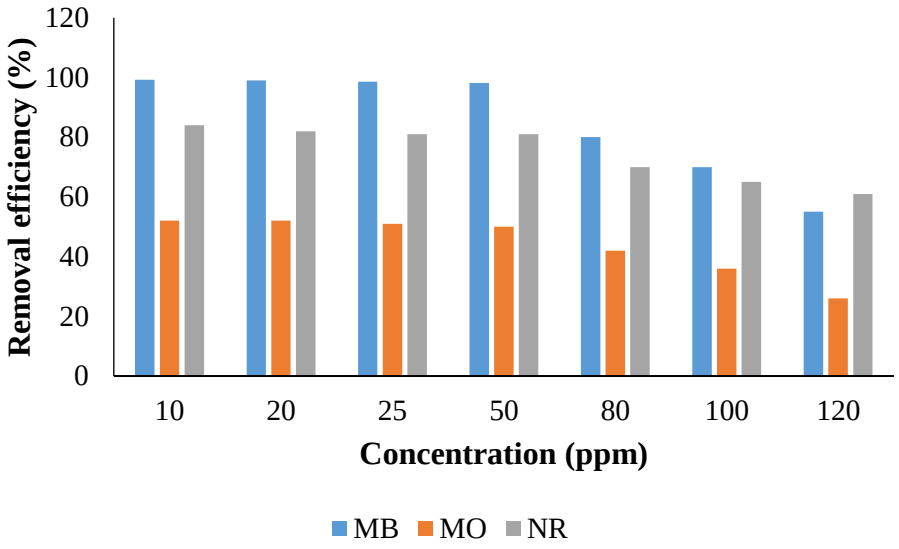

Fig. 4.9 Removal efficiency of MB, MO and NR dyes using SCB with variable initial concentrations of MB dye. (Adsorbent dose: 8 g L^{-1}, contact time: 120 min, and pH: 10-MB, 8-NR, 12-MO)

4.9 Adsorption kinetics and isotherm models

Optimisation of contact time is important for the adsorption examination to confirm complete equilibrium between the dyes (MB, MO and NR) and SCB adsorbent. The pseudo-first-order (PFO) and pseudo-second-order (PSO) model adsorption kinetics were investigated to propose a plausible kinetic mechanism. Table 4.1 depicts the different parameters of the PFO and PSO adoption kinetics for the adsorption of different dyes (MB, MO and NR) on SCB adsorbent. The correlation coefficient (R^2) values for PFO and PSO models were 0.9319 and 0.9994, respectively, for MB dye adsorption on SCB material. The R^2 values for the PFO and PSO

models were 0.634 and 0.9912, respectively, for MO dye adsorption on SCB material. The correlation coefficient (R^2) for PFO and PSO models were 0.9251 and 0.9988, respectively, for NR dye adsorption on SCB material. The R^2 value for PFO was far more than unity compared to the PSO model, indicating the PSO linear second-order model fitting for the adsorption of MB dye SCB adsorbent. The PSO model fitting established chemical adsorption, P. Das & Debnath (2022). These values of the PSO model compared to the PFO model were due to the smaller difference between the experimental and theoretical values for the PSO and PFO models (Fig. 4.10).

PFO-MB

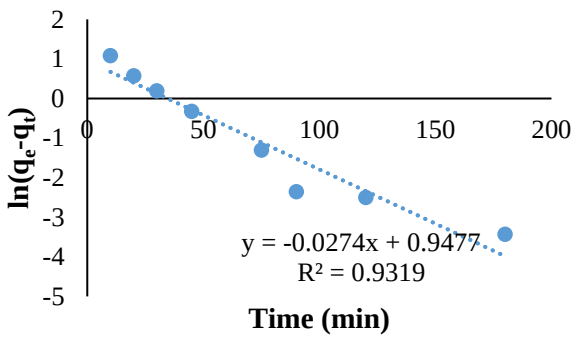

PSO-MB

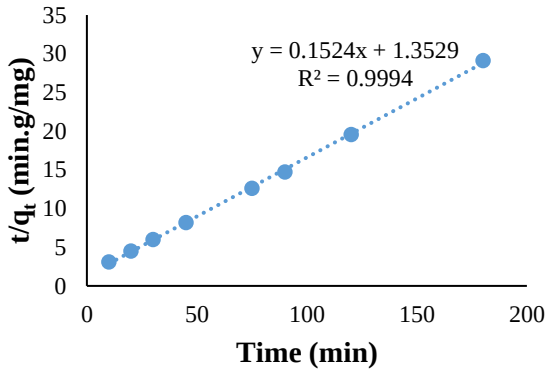

PFO-NR

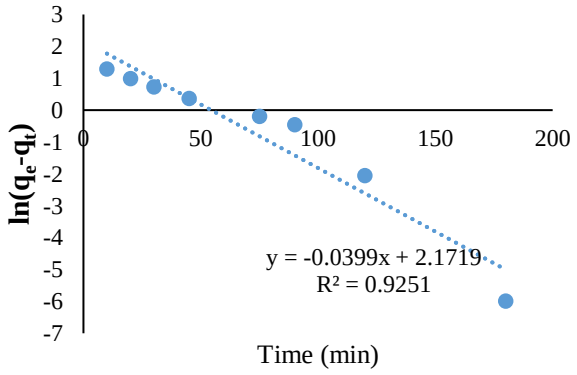

PSO-NR

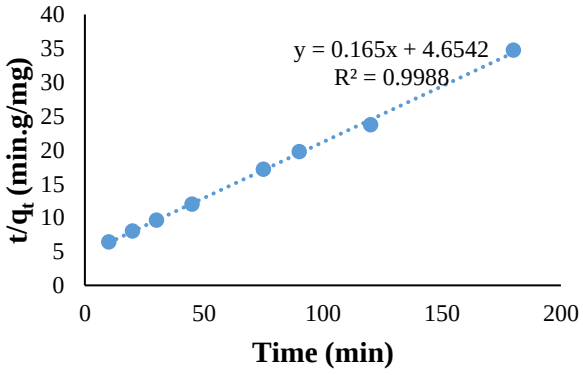

PFO-MO

PSO-MO

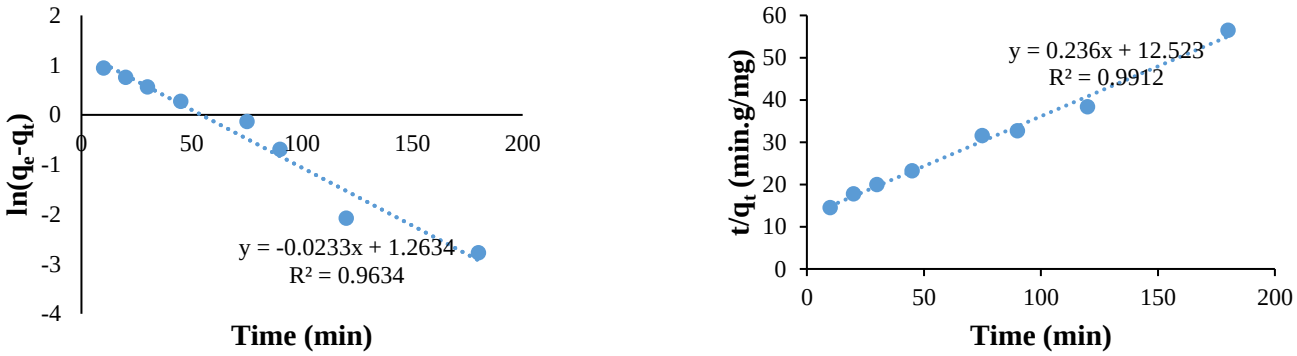

Fig. 4.10 Linear form of PFO and PSO kinetic isotherms

Table 4.1 PFO and PSO kinetics' parameter for dye adsorption on SCB

	MB		**NR**		**MO**	
	PFO	**PSO**	**PFO**	**PSO**	**PFO**	**PSO**
Intercept	0.948	1.353	1.263	12.523	2.172	4.654
Slope	-0.027	0.152	-0.023	0.236	-0.04	0.165
q_e **(mg g^{-1})**	2.58	6.562	3.537	4.237	8.775	6.061
k1 **(min^{-1})**	-0.0002	0.017	-0.0001	0.004	-0.0002	0.006
R^2	0.932	0.999	0.963	0.991	0.925	0.999

The current study examined two adsorption isotherms (Freundlich and Langmuir) for the adsorption of MB dye on SCB adsorbent. The regression coefficient (R^2), reduced chi-square, and residual sum of the square were assessed to distinguish between two isotherm models (Table 4.2). The R^2 value was close to unity for the Langmuir model (Freundlich: 0.8405 and Langmuir: 0.9933) for MB dye adsorption on SCB adsorbent. The R^2 value was suitable for fitting with the Langmuir isotherm model for MB dye adsorption on SCB adsorbent. If the value of KL is between 0 and 1, the system is considered suitable for adsorption purposes; for the present study, the value of n was 18, indicating the SCB adsorbent is suitable for MB dye adsorption. Moreover, the experimental data and predicted results obtained for the MB dye

adsorption on SCB adsorbent were found in close correlation (R^2= 0.9933), making this model applicable to the present work. A typical Langmuir isotherm shows a characteristic horizontal asymptote, indicating saturation after the monolayer adsorption. This showed that the dye's adsorption mechanism on SCB adsorbent was chemisorption. The closeness of experimental and predicted data points was also examined (Fig. 4.11).

Langmuir-MB

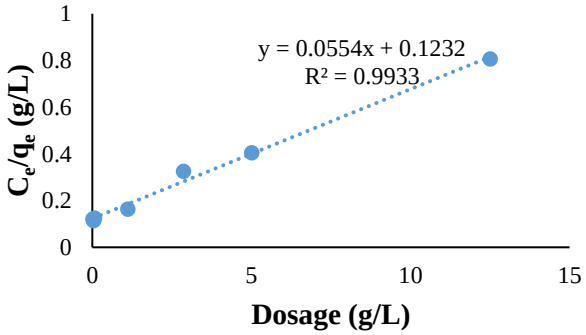

Freundlich-MB

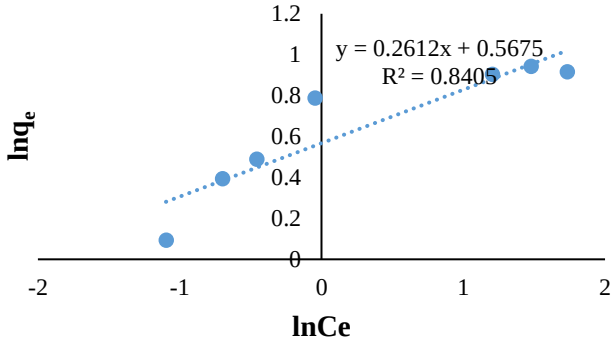

Langmuir-NR

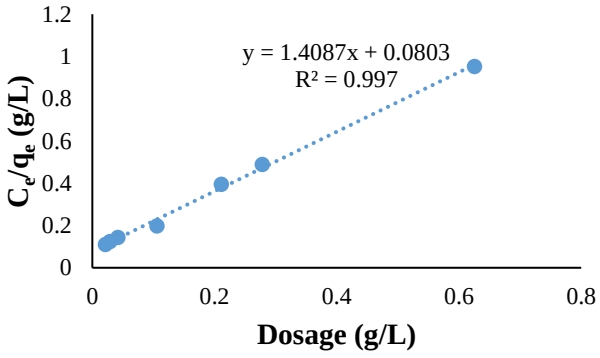

Freundlich-NR

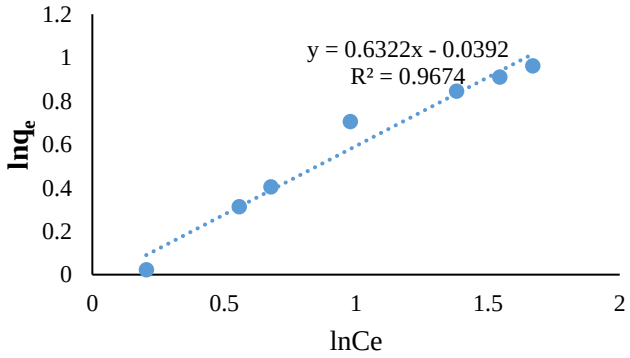

Langmuir-MO

Freundlich-MO

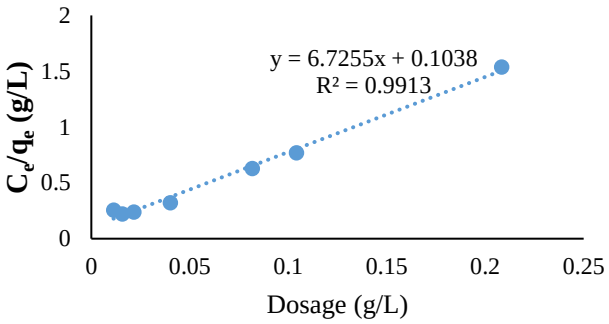

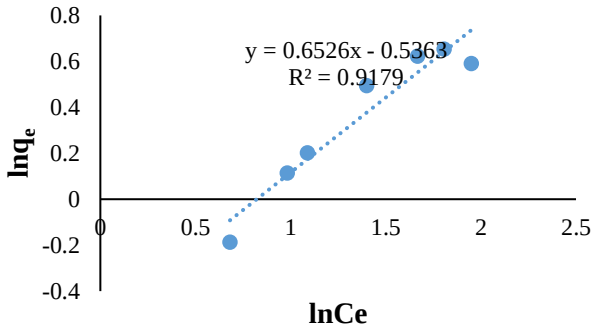

Fig. 4.11 The linear form of Freundlich and Langmuir adsorption isotherms

Table 4. 2 Freundlich and Langmuir isotherm's parameter for dye adsorption on SCB

	MB		**NR**		**MO**	
	Freundlich	**Langmuir**	**Freundlich**	**Langmuir**	**Freundlich**	**Langmuir**
Intercept	0.568	0.123	-0.039	0.0803	-0.536	0.104
Slope	0.261	0.055	0.632	1.4087	0.653	6.72
K	6.746	1.131	0.962	8.84	0.585	1.432
n	-	18.051	1.582		1.532	-
R²	0.841	0.993	0.967	0.997	0.918	0.991

This research synthesised treated SCB using the process described in earlier sections. The total cost (USD) of manufacturing 1.0 kg chemically treated SCB was USD 3.1.

4.10 Conclusions

Even though sugarcane bagasse has been widely utilised for the adsorption of several dyes, the simultaneous adsorption of anionic, cationic and neutral dyes using sugarcane bagasse hasn't been done by anyone before as well as there are only a few researches on the adsorption of anionic and even fewer on neutral dyes. This study presents the use of low-cost chemically treated sugarcane bagasse for the adsorption of three dyes: cationic MB, MO and NR dyes. The

prepared SCB was characterised using a scanning electron microscope (morphology) and FTIR techniques. The total cost (USD) of manufacturing 1.0 kg chemically treated SCB was USD 3.1. The FTIR spectra revealed that all the bands, due to the presence of cellulose, pectin, and lignin, were identified in the sugarcane bagasse. The effect of adsorbent dose, contact time, pH, and concentration on the adsorption performance of sugarcane bagasse for the removal of MB, MO, and NR dyes was studied. Kinetic and isotherm studies were also carried out to further study the adsorption process. The maximum adsorptive removal efficiency of MB, MO and NR dyes was found to be 98.2%, 50.3% and 81.2%, respectively, at the optimised condition of adsorbent dose: 8 g/L, time: 120 min, pH: pH: 10-MB, 8-NR, 12-MO and concentration: 50 ppm. From adsorption kinetics, it was established that the adsorption process followed pseudo-second-order rather than pseudo-first-order. The correlation coefficient values for the PFO and PSO models were 0.9319 and 0.9994, respectively, for MB dye adsorption on SCB. The adsorption isotherm study established that the adsorption process followed the Langmuir model rather than the Freundlich model. This study established that a waste material such as SCB can be a good adsorbent for textile wastewater treatment.

4.11 References

Abdelghaffar, F., Abdelghaffar, R. A., Mahmoud, S. A., & Youssef, B. M. (2019). Modified sugarcane bagasse for the removal of anionic dyes from aqueous solution. Pigment & Resin Technology, 48(5), 464–471. https://doi.org/10.1108/prt-01-2019-0003

Amin, N. K. (2008). Removal of reactive dye from aqueous solutions by adsorption onto activated carbons prepared from sugarcane bagasse pith. Desalination, 223(1–3), 152–161. https://doi.org/10.1016/j.desal.2007.01.203

Arni, S. A. (2018). Extraction and isolation methods for lignin separation from sugarcane bagasse: A review. Industrial Crops and Products, 115, 330–339.

https://doi.org/10.1016/j.indcrop.2018.02.012

Bai, L., Su, X., Feng, J., & Ma, S. (2021). Preparation of sugarcane bagasse biochar/nano-iron oxide composite and mechanism of its Cr (VI) adsorption in water. Journal of Cleaner Production, 320, 128723. https://doi.org/10.1016/j.jclepro.2021.128723

Benkhaya, S., Rabet, S. M., & Harfi, A. E. (2020). A review on classifications, recent synthesis and applications of textile dyes. Inorganic Chemistry Communications, 115, 107891. https://doi.org/10.1016/j.inoche.2020.107891

Berizi, Z., Hashemi, S. Y., Hadi, M., Azari, A., & Mahvi, A. H. (2016). The study of non-linear kinetics and adsorption isotherm models for Acid Red 18 from aqueous solutions by magnetite nanoparticles and magnetite nanoparticles modified by sodium alginate. Water Science & Technology, 74(5), 1235–1242. https://doi.org/10.2166/wst.2016.320

Berradi, M., Hsissou, R., Khudhair, M., Assouag, M., Cherkaoui, O., Bachiri, A. E., & Harfi, A. E. (2019). Textile finishing dyes and their impact on aquatic environs. Heliyon, 5(11), e02711. https://doi.org/10.1016/j.heliyon.2019.e02711

Biswal, H. J., Yadav, A., Vundavilli, P. R., & Gupta, A. (2021). High aspect ZnO nanorod growth over electrodeposited tubes for photocatalytic degradation of EtBr dye. RSC Advances, 11(3), 1623–1634. https://doi.org/10.1039/d0ra08124h

Brienzo, M., Siqueira, A., & Milagres, A. (2009). Search for optimum conditions of sugarcane bagasse hemicellulose extraction. Biochemical Engineering Journal, 46(2), 199–204. https://doi.org/10.1016/j.bej.2009.05.012

Chiao, Y., Chen, S., Sivakumar, M., Ang, M. B. M. Y., Patra, T., Almodovar, J., Wickramasinghe, S. R., Hung, W., & Lai, J. (2020). Zwitterionic Polymer Brush Grafted on Polyvinylidene Difluoride Membrane Promoting Enhanced Ultrafiltration Performance with Augmented Antifouling Property. Polymers, 12(6), 1303.

https://doi.org/10.3390/polym12061303

Da Silva, L. G., Ruggiero, R., De M Gontijo, P., Pinto, R. B., Royer, B., Lima, E. C., Fernandes, T. H., & Calvete, T. (2011). Adsorption of Brilliant Red 2BE dye from water solutions by a chemically modified sugarcane bagasse lignin. Chemical Engineering Journal, 168(2), 620–628. https://doi.org/10.1016/j.cej.2011.01.040

Das, P., & Debnath, A. (2022). Fabrication of MgFe 2 O 4 /polyaniline nanocomposite for amputation of methyl red dye from water: Isotherm modeling, kinetic and cost analysis. Journal of Dispersion Science and Technology, 44(14), 2587–2598. https://doi.org/10.1080/01932691.2022.2110110

Das, S., Pal, A., & Debnath, A. (2023). Polyaniline-Coated Magnesium Ferrite Nanocomposite: Synthesis, Characterization, Fabrication Cost Analysis and Dye Sorption Behavior with Scale-Up Design. ChemistrySelect, 8(29). https://doi.org/10.1002/slct.202300928

Das, S., Paul, S. R., & Debnath, A. (2023). Fabrication of biochar from jarul (Lagerstroemia speciosa) seed hull for ultrasound aided sequestration of ofloxacin from water: Phytotoxic assessments and cost analysis. Journal of Molecular Liquids, 387, 122610. https://doi.org/10.1016/j.molliq.2023.122610

Deb, A., Das, S., & Debnath, A. (2023). Fabrication and characterization of organometallic nanocomposite for efficient abatement of dye laden wastewater: CCD optimization, adsorption mechanism, co-existing ions, and cost analysis. Chemical Physics Letters, 830, 140820. https://doi.org/10.1016/j.cplett.2023.140820

Dindorkar, S. S., Patel, R. V., & Yadav, A. (2022). Adsorptive removal of methylene blue dye from aqueous streams using photocatalytic CuBTC/ZnO chitosan composites. Water Science & Technology, 85(9), 2748–2760. https://doi.org/10.2166/wst.2022.142

Dutta, S., Gupta, B., Srivastava, S. K., & Gupta, A. K. (2021). Recent advances on the

removal of dyes from wastewater using various adsorbents: a critical review. Materials Advances, 2(14), 4497–4531. https://doi.org/10.1039/d1ma00354b

Fakher, S., & Imqam, A. (2019). A review of carbon dioxide adsorption to unconventional shale rocks methodology, measurement, and calculation. SN Applied Sciences, 2(1). https://doi.org/10.1007/s42452-019-1810-8

Feng, Y., Cheng, T., Yang, W., Ma, P., He, H., Yin, X., & Yu, X. (2017). Characteristics and environmentally friendly extraction of cellulose nanofibrils from sugarcane bagasse. Industrial Crops and Products, 111, 285–291. https://doi.org/10.1016/j.indcrop.2017.10.041

Gajera, R., Patel, R. V., Yadav, A., & Labhasetwar, P. K. (2022). Adsorption of cationic and anionic dyes on photocatalytic flyash/TiO2 modified chitosan biopolymer composite. Journal of Water Process Engineering, 49, 102993. https://doi.org/10.1016/j.jwpe.2022.102993

Garside, P., & Wyeth, P. (2003). Identification of cellulosic fibres by FTIR spectroscopy - thread and single fibre analysis by attenuated total reflectance. Studies in Conservation, 48(4), 269–275. https://doi.org/10.1179/sic.2003.48.4.269

Geng, Y., Zhang, J., Zhou, J., & Lei, J. (2018). Study on adsorption of methylene blue by a novel composite material of TiO2 and alum sludge. RSC Advances, 8(57), 32799–32807. https://doi.org/10.1039/c8ra05946b

Jahan, K., Tyeb, S., Kumar, N., & Verma, V. (2020). Bacterial Cellulose-Polyaniline Porous Mat for Removal of Methyl Orange and Bacterial Pathogens from Potable Water. Journal of Polymers and the Environment, 29(4), 1257–1270. https://doi.org/10.1007/s10924-020-01947-w

Kerrou, M., Bouslamti, N., Raada, A., Elanssari, A., Mrani, D., & Slimani, M. S. (2021). The Use of Sugarcane Bagasse to Remove the Organic Dyes from Wastewater. International

Journal of Analytical Chemistry, 2021, 1–11. https://doi.org/10.1155/2021/5570806

Kharat, D. S. (2015). PREPARING AGRICULTURAL RESIDUE BASED ADSORBENTS FOR REMOVAL OF DYES FROM EFFLUENTS - A REVIEW. Brazilian Journal of Chemical Engineering, 32(1), 1–12. https://doi.org/10.1590/0104-6632.20150321s00003020

Koduru, J. R., Karri, R. R., & Mubarak, N. M. (2019). Smart materials, magnetic graphene Oxide-Based nanocomposites for sustainable water purification. In Springer eBooks (pp. 759–781). https://doi.org/10.1007/978-3-030-05399-4_26

Kumar, A., Negi, Y. S., Choudhary, V., & Bhardwaj, N. K. (2020a). Characterization of Cellulose Nanocrystals Produced by Acid-Hydrolysis from Sugarcane Bagasse as Agro-Waste. Journal of Materials Physics and Chemistry, 2(1), 1–8. https://doi.org/10.12691/jmpc-2-1-1

Kumar, A., Negi, Y. S., Choudhary, V., & Bhardwaj, N. K. (2020b). Characterization of Cellulose Nanocrystals Produced by Acid-Hydrolysis from Sugarcane Bagasse as Agro-Waste. Journal of Materials Physics and Chemistry, 2(1), 1–8. https://doi.org/10.12691/jmpc-2-1-1

Kurniawati, D., Bahrizal, N., Sari, T. K., Adella, F., & Sy, S. (2021). Effect of Contact Time Adsorption of Rhodamine B, Methyl Orange and Methylene Blue Colours on Langsat Shell with Batch Methods. Journal of Physics Conference Series, 1788(1), 012008. https://doi.org/10.1088/1742-6596/1788/1/012008

Lellis, B., Fávaro-Polonio, C. Z., Pamphile, J. A., & Polonio, J. C. (2019). Effects of textile dyes on health and the environment and bioremediation potential of living organisms. Biotechnology Research and Innovation, 3(2), 275–290. https://doi.org/10.1016/j.biori.2019.09.001

Lin, J., & Wang, L. (2009). Comparison between linear and non-linear forms of pseudo-first-order and pseudo-second-order adsorption kinetic models for the removal of methylene blue by activated carbon. Frontiers of Environmental Science & Engineering in China, 3(3), 320–324. https://doi.org/10.1007/s11783-009-0030-7

Mate, C. J., & Mishra, S. (2020). Synthesis of borax cross-linked Jhingan gum hydrogel for remediation of Remazol Brilliant Blue R (RBBR) dye from water: Adsorption isotherm, kinetic, thermodynamic and biodegradation studies. International Journal of Biological Macromolecules, 151, 677–690. https://doi.org/10.1016/j.ijbiomac.2020.02.192

Noreen, S., Bhatti, H. N., Iqbal, M., Hussain, F., & Sarim, F. M. (2020). Chitosan, starch, polyaniline and polypyrrole biocomposite with sugarcane bagasse for the efficient removal of Acid Black dye. International Journal of Biological Macromolecules, 147, 439–452. https://doi.org/10.1016/j.ijbiomac.2019.12.257

Oudiani, A. E., Chaabouni, Y., Msahli, S., & Sakli, F. (2011). Crystal transition from cellulose I to cellulose II in NaOH treated Agave americana L. fibre. Carbohydrate Polymers, 86(3), 1221–1229. https://doi.org/10.1016/j.carbpol.2011.06.037

Patel, R. V., Raj, G. B., Chaubey, S., & Yadav, A. (2022). Investigation on the feasibility of recycled polyvinylidene difluoride polymer from used membranes for removal of methylene blue: experimental and DFT studies. Water Science & Technology, 86(1), 194–210. https://doi.org/10.2166/wst.2022.193

Patel, R. V., & Yadav, A. (2021). Photocatalytic MIL101(Fe)/ZnO chitosan composites for adsorptive removal of tetracycline antibiotics from the aqueous stream. Journal of Molecular Structure, 1252, 132128. https://doi.org/10.1016/j.molstruc.2021.132128

Ponce, J., Da Silva Andrade, J. G., Santos, L. N. D., Bulla, M. K., Barros, B. C. B., Favaro, S. L., Hioka, N., Caetano, W., & Batistela, V. R. (2021). Alkali pretreated sugarcane bagasse, rice husk and corn husk wastes as lignocellulosic biosorbents for dyes.

Carbohydrate Polymer Technologies and Applications, 2, 100061. https://doi.org/10.1016/j.carpta.2021.100061

Prasad, L., Kumar, S., Patel, R. V., Yadav, A., Kumar, V., & Winczek, J. (2020). Physical and mechanical behaviour of sugarcane bagasse Fibre-Reinforced Epoxy Bio-Composites. Materials, 13(23), 5387. https://doi.org/10.3390/ma13235387

Saha, B., Shaji, S., & Debnath, A. (2023). Fabrication of polyaniline-based calcium ferrite nanocomposite and its application in sequestration of Victoria blue dye from wastewater. Journal of Dispersion Science and Technology, 1–15. https://doi.org/10.1080/01932691.2023.2273432

Sahu, N., Rawat, S., Singh, J., Karri, R. R., Lee, S., Choi, J., & Koduru, J. R. (2019). Process Optimization and Modeling of Methylene Blue Adsorption Using Zero-Valent Iron Nanoparticles Synthesized from Sweet Lime Pulp. Applied Sciences, 9(23), 5112. https://doi.org/10.3390/app9235112

Segal, L., Creely, J., Martin, A., & Conrad, C. (1959). An empirical method for estimating the degree of crystallinity of native cellulose using the X-Ray diffractometer. Textile Research Journal, 29(10), 786–794. https://doi.org/10.1177/004051755902901003

Tahir, H., Sultan, M., Akhtar, N., Hameed, U., & Abid, T. (2012). Application of natural and modified sugar cane bagasse for the removal of dye from aqueous solution. Journal of Saudi Chemical Society, 20, S115–S121. https://doi.org/10.1016/j.jscs.2012.09.007

Viera, R. G., Filho, G. R., De Assunção, R. M., Da S Meireles, C., Vieira, J. G., & De Oliveira, G. S. (2006). Synthesis and characterization of methylcellulose from sugar cane bagasse cellulose. Carbohydrate Polymers, 67(2), 182–189. https://doi.org/10.1016/j.carbpol.2006.05.007

Wang, R., Deng, L., Li, K., Fan, X., Li, W., & Lu, H. (2020). Fabrication and

characterization of sugarcane bagasse–calcium carbonate composite for the efficient removal of crystal violet dye from wastewater. Ceramics International, 46(17), 27484–27492. https://doi.org/10.1016/j.ceramint.2020.07.237

Yu, J., Chi, R., Zhang, Y., Xu, Z., Xiao, C., & Guo, J. (2012). A situ co-precipitation method to prepare magnetic PMDA modified sugarcane bagasse and its application for competitive adsorption of methylene blue and basic magenta. Bioresource Technology, 110, 160–166. https://doi.org/10.1016/j.biortech.2012.01.134

Zhang, Z., Moghaddam, L., O'Hara, I. M., & Doherty, W. O. (2011). Congo Red adsorption by ball-milled sugarcane bagasse. Chemical Engineering Journal, 178, 122–128. https://doi.org/10.1016/j.cej.2011.10.024